Crazing Micromechanism in Glassy Atactic Polystyrene and Its Blends with Poly(2,6-dimethyl-1,4-diphenyl oxides) by AFM

J.-H. Lin and A. C.-M. Yang*

Department of Materials Science and Engineering, National Tsing Hua University, Hsinchu, Taiwan

Received August 3, 2000; Revised Manuscript Received February 12, 2001

ABSTRACT: Crazing in glassy polymer thin films was found to follow a micronecking process similar to that of local shear deformation in ductile polymers. The void fraction in the fully necked craze region was determined, and a close-packed fibril structure was concluded. The local stress and strain within the craze were obtained from AFM topographic data by the Bridgman's plasticity analysis. The stress/strain curve of craze fibrillation was subsequently determined where an apparent strain softening was found in the initiation of fibrillation, which was then followed by strain hardening as fibrils were drawn into the neck region. Strain rate was found to peak at the craze boundaries, consistent with the surface drawing mechanism from TEM results. During craze fibrillation, the local strain rate of the drawn polymer increased with drawing strain until a critical strain ϵ_h was reached; beyond that, the strain rate decreased with the strain. The critical strain ϵ_h, identified as the onset of strain hardening, was found to decrease with entanglement density ν_e in the low-ν_e, craze-forming regime but become a constant in the high-ν_e regime where crazing was replaced by shear yielding. The transition between crazing and shearing is controlled by the tendency of strain localization in the entanglement network.

1. Introduction

The brittle nature of glassy polymers has always been a fatal drawback for extensive and novel applications. This brittleness can be traced to the formation of the microscopic crazes during plastic deformation.[1−23] The nucleation of craze is believed to result from the local strain softening at the heterogeneously strained sites, where the strain softening characteristic leads to both an acceleration of the strain rate and a localization of strain in these areas. The growth of craze can be divided into two mechanisms at the craze tip and the craze−matrix boundaries: the craze tip advancement and craze thickening, respectively. A widely accepted hypothesis[7] on the craze tip advancement is that the craze tip breaks up into a series of void fingers by the Taylor meniscus instability.[15,24−26] As the fingerlike craze tip structure propagates, fibrils develop by deformation of the polymer webs between the fingers. Following the deduction and assumption of Fields and Ashby,[7,26] the advance velocity of the craze tip at the steady state can be represented by the equation

$$v_0 \approx \frac{\sqrt{3}}{2}\frac{\dot{\epsilon}_f h}{n+2}\left[\frac{\sqrt{3}h(\beta^* S_t)^2}{8\sigma_f \Gamma}\right]^2\left(1-\frac{2\Gamma}{\beta^* S_t h}\right)^{2n}$$

where h is the thickness of the craze behind the craze tip, $\beta^* S_t$ is the hydrostatic stress midway between void fingers, Γ is the surface energy, n is the non-Newtonian flow law exponent, and σ_f, $\dot{\epsilon}_f$ are material parameters. The important conclusion is that the advancing velocity of craze tip is very sensitive to the energy Γ of the surface being created.

Almost concurrent to the craze tip advancement, at the craze−matrix interface craze thickening occurs, during which new material is drawn into the craze from the elastic region. The drawing mechanism has a property that the volume fraction of polymer in the craze is approximately constant.[9] The most important parameter for traditional mechanical analysis of the micromechanism is the normal tensile stress, $S(x)$, which is measured by the craze surface displacement profile along the craze and then used to compute the $S(x)$ profile. For simplicity, the polymer outside the craze is assumed to be under linear elastic deformation, and the dislocation method of stress analysis is used to determine craze stress fields.[27] The stress $S(x)$ can be expressed as[11,13,14,27]

$$S(x) = \frac{E^* b}{2\pi} x\sqrt{x^2 - c^2}\int_c^\alpha \frac{\mathrm{d}x_1\, \alpha(x_1)}{\sqrt{x_1^2 - c^2(x^2 - x_1^2)}}$$

where $E^* = E/(1-\nu^2)$ in which ν is the Poisson ratio, b is the Burger vector of the array of continuously distributed dislocations which are used to model the behavior of craze, c and a are the half lengths of the crack and the total defect (crack and craze combined), respectively, $\alpha(x)$ is the dislocation density, and x is the distance away from crack. In this way, the stress distribution along the longitudinal direction of the craze can be obtained and analyzed in detail.

The microstructure of craze has been studied extensively, especially in thin film specimens by TEM.[16−21] It was found to consist of microfibrils and microvoids. Through small-angle X-ray scattering (SAXS) and low-angle electron diffraction (LAED) techniques, the average diameter and the arrangement of these microfibrils have been determined.[5,8,18,28,29] The draw ratio in the crazed region was measured by the TEM microdensitometry technique.[9,10,19−21] The remarkable draw ratio of around 400% in the crazed region is much greater than the fracture elongation (ca. 1−2%) in bulk glassy polymers. Later, Yang utilized the method of atomic force microscopy (AFM) to study the crazes in polymer thin films and found that the crazed region was depressed with a saturated depth of one-third of the film thickness.[22] The depression was concluded as the result of micronecking during the crazing process. This micronecking mechanism induces the formation of crazes

10.1021/ma001367r CCC: $20.00
Published on Web 04/19/2001

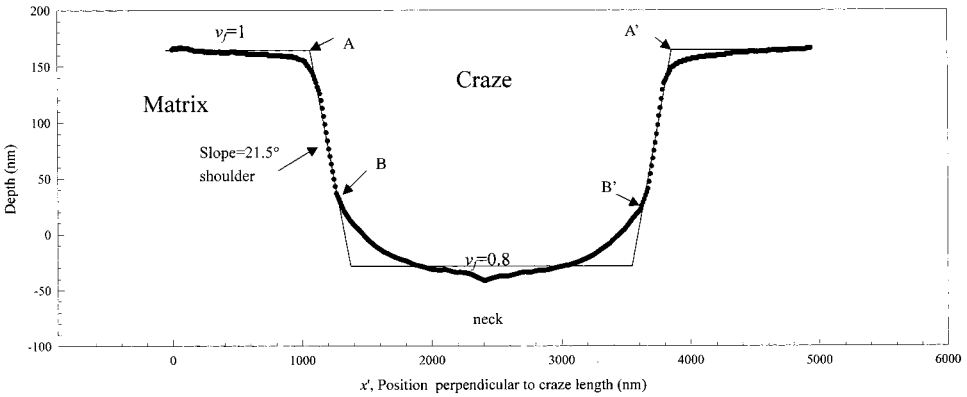

Figure 1. An AFM topographic profile of crazes in a 0.45 μm thick PS film.

as well as the other types of strain localization in polymers, e.g., shear deformation zones in ductile glassy polymers during deformation. According to the calculation of the Bridgman model,[30] there is an additional triaxial tension stress and shear stress induced during the formation of the necking process. By this classical calculation, we can analyze the stress distribution at the necking area.[22,30] In this paper, the micromechanical data of stress, strain, and strain rate that associated with crazing in glassy polymer thin films were studied by using AFM and the mechanical models.

2. Experimental Procedures

The polystyrene (PS) was purchased from the Pressure Chemical Co. with molecular weight dispersity $M_w/M_n = 1.06$. The poly(phenylene oxide) (PPO) was obtained from Aldrich Chemical Co. with a molecular weight of 244 000. The polymer thin film was prepared by solution-casting the toluene solution in a spin coater at spin speed of 1500 rpm. The film thickness was controlled to be around 0.45 μm. When the solvent evaporated, the PS film was floated onto a water surface and picked up on a piece of copper grids. After proper bonding procedure,[9] the specimen was mounted in a strain jig and stretched under an optical microscope to observe the growth of local deformation zones (crazes or shear deformation zones). The applied strain rate was restricted within the range of $10^{-4}-10^{-5}$/s. For investigating the molecular weight effect, several molecular weights of PS were used including 90K, 200K, 900K, 2M, and 30M, with film thickness 0.45 μm. For the entanglement density effect, the PS ($M_w = 2$M) and poly(phenylene oxide) (PPO) ($M_w = 24\,400$) were separately blended with the PS oligomer diluents ($M_w = 2$K) to adjust entanglement densities. The high molecular weight compositions and corresponding entanglement densities of the miscible blends were 100% PPO (15×10^{25} chains/m^3), 90% PPO (12×10^{25} chains/m^3), 70% PPO (7.35×10^{25} chains/m^3), 100% PS (3.3×10^{25} chains/m^3), 90% PS (2.67×10^{25} chains/m^3), and 70% PS (1.62×10^{25} chains/m^3).

The stretched PS film samples were then examined under an AFM (Digital Instrumental, Nanoscope IIIa) to investigate the topographic information on the local deformation zones. The AFM topographic data were used to calculate the local micromechanical information in the crazes using an in-house developed software to simplify the tedious work of calculation.

3. Results and Discussion

I. Micronecking Mechanism of the Craze. It is well-known that the brittle PS thin film crazes at around 1% strain. The AFM topographic profile of the craze is illustrated in Figure 1. Clearly demonstrated, the crazed region is depressed. The AFM craze profile was divided into the neck and the shoulder regions. The shoulder region is defined as the area between the cross-section points A (or A′) and B (or B′), as depicted in Figure 1. On the other hand, the neck region is the central region between points B and B′. Being the steepest section of the AFM craze topography, the profile of the shoulder has a maximum surface angle θ (of the sections AB and A′B′) around 21.5°, well below the AFM tip angle, which varies with the scan direction[22] of around 40°−65°. Consequently, the AFM profile represents the true craze topography. As shown later in the next section, the craze depth increases linearly with craze width but saturates when the craze width is greater than approximately 2.5 μm for the 0.45 μm thick PS film. As concluded previously,[22] the surface depression in the craze region is a result of micronecking during the strain localization process, which is similar to, but on a very different scale from, that occurring during the cold drawing of glassy polymers.[31] Therefore, only mature craze sections, where craze width is greater than 2.5 μm, were examined for a complete study of the microdrawing process of crazing.

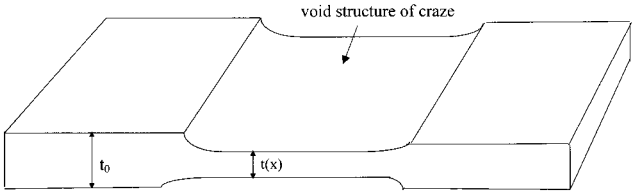

Figure 2. A schematic drawing of the micronecking associated with crazing.

It is interesting that from the apparent AFM topographic profile the tensile strain ϵ in the craze can be calculated as a function of position within the craze. As a preliminary calculation, it is assumed that the necking produces no volume change whereas the voids volume underneath the AFM craze topography is neglected. Under these circumstances, the local strain $\epsilon(x)$ can be calculated from the apparent thickness reduction[32] by

$$\epsilon(x) = \ln[A_0/A(x)] = 2\ln[t_0/t(x)]$$

where A_0, t_0, $A(x)$, and $t(x)$ are the original film cross-sectional area, original film thickness, the film cross-sectional area in the craze, and the film thickness within the craze, respectively; these parameters are illustrated in Figure 2. Figure 3 shows the calculated strain from a mature craze. A plateau of elevated strain in the middle region of the craze, i.e., the neck region, is evident. The maximum elevated strain according to this preliminary calculation is around 220% (Figure 3), resulting in a craze fibril extension ratio λ of approximately 3.2 ($\lambda \equiv 1 + \epsilon$) and a craze volume fraction

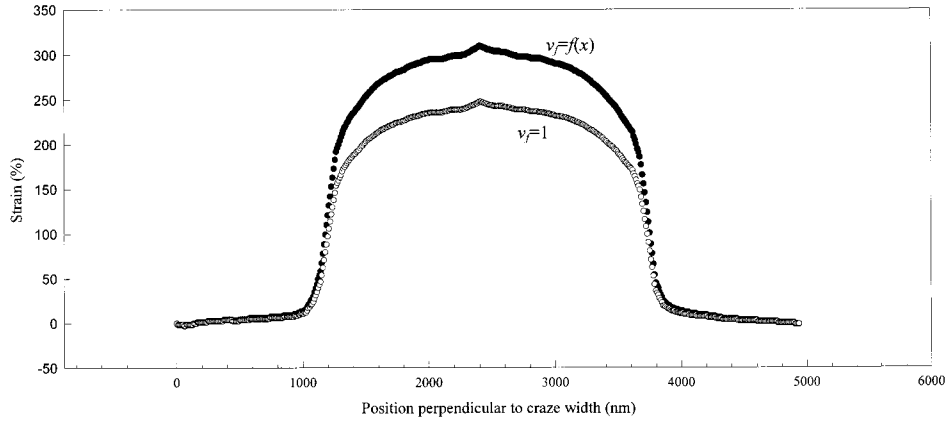

Figure 3. Local tensile strain distribution across the craze width.

V_f (relative to the original film thickness t_0) of 0.31 since, according to Kramer,[1] $V_f = \lambda^{-1}$. This value 0.31 is significantly greater than the 0.25 measured by TEM microdensitometry.[1] Apparently, this discrepancy results from the void content v_v in the neck, which is difficult to detect accurately with the conventional AFM method. The fact that the internal craze structure may be different from that of the surface is due to possible fibril coalescence,[18] which further increases the degree of infeasibility. Hence, the TEM result was used to calibrate the void fraction v_v in the neck. The calibration was carried out using $v_v = (V_{f,AFM} - V_{f,TEM})/V_{f,AFM}$ gives $v_v = 0.2$ and the packing density of fibrils in the neck, $v_f = 1 - v_v$, to be approximately 0.8, which is very close to the theoretical maximum packing density of cylinders, around 0.79. This result is reasonable as the fully fibrillated craze fibrils,[1] when entering the central neck region, would inevitably be highly compressed into maximum packing as a result of maximal thickness contraction associated with necking. It can be readily shown that $v_f = V_{f,TEM}/V_{f,AFM}$ indicates that v_f is the degree of contraction of the craze fibrils in the thickness direction.

Taking into account the voids volume in the craze, the strain in the craze $\epsilon(x)$ can be calculated from the AFM craze topography and the packing density $v_f(x)$ by

$$\epsilon(x) = \ln[A_0/A(x)] = 2\ln[t_0/t(x)v_f^{1/3}(x)] = 2\ln[t_0/t(x)] - {}^2/_3\ln[v_f(x)]$$

At the neck, with v_f taken as a constant equal to 0.8, the maximum strain is calibrated to be approximately 300%, significantly greater than the uncalibrated value of 220%. Furthermore, for the shoulder regions at the both sides of the neck, the fibril packing density v_f is very difficult to access due to the inability to obtain simultaneous AFM and TEM data at the narrow region (ca. <0.3 μm width). As an approximation, the fibril packing density $v_f(x)$ is assumed to decrease linearly with the distance x from the craze/matrix boundary from $v_f = 1$ in the matrix to $v_f = 0.8$ in the neck (as shown in Figure 1). The strain in the craze $\epsilon(x)$ was calculated, and the result is also shown in Figure 3. The curve demonstrates a similar behavior where it increases rapidly at the shoulder region and then reaches a maximum strain in the neck region although the calibrated strain is generally higher than the uncalibrated strain.

II. Stress Distribution in the Crazed Region. The stress distribution in the necked area can be calculated by classical necking mechanics. Following Bridgman,[30] for force balance of a necking plate, as depicted in Figure 3, the integration of the tensile stress at any cross section of the specimen should be equal to the applied load, i.e.,

$$\int_0^a \sigma_{zz}\,\mathrm{d}r = F_{zz}$$

where σ_{zz} is the tensile stress along the loading axial, r is the distance away from the neutral axis, a is the distance from the neutral axis to the surface of the specimen, and F_{zz} is the applied load along the tensile axis. When necking initiates, there is a hydrostatic tension σ_{rr} induced at the site of necking area which can be expressed as

$$\sigma_{rr} = F\log\left(\frac{a^2 + 2aR - r^2}{2aR}\right)$$

where R is the local surface curvature at the neck. In addition to the triaxial tension induced at the necked site, a surface shear stress τ is operative at the surface of the neck region,

$$\tau = \sigma_{rr}/\cos^2\alpha$$

where α is the local surface angle between the surface and stretching axis. The local topographic data of α, r, R, and a can be readily obtained from AFM scanning the craze surface from which the stress distribution within a craze can be calculated directly. The stress distribution calculated from the AFM topography corrected with the fibril packing density $v_f(x)$ is shown in Figure 4. Stress distribution inside the craze is higher than that in the elastic deformed region and demonstrates a maximum stress located at the central region of the crazes, caused by the largest cross-sectional area reduction in this region. The maximum stress in craze is roughly 4.2 times greater than the outside craze and approximately 1.43 times of the raw data without calibration. The shear stress across a craze can also be calculated using the Bridgman equation. The shear stress also concentrates in the crazed region with a marked maximum at each craze/matrix boundary. Shown later, the high shear stress at the edge of the craze is responsible for fibril drawing.

III. Microdrawing Process during Crazing. The formation of the craze is always a consequence of the strain localization. Under the traditional testing approach, it is hard to obtain the microscopic stress and

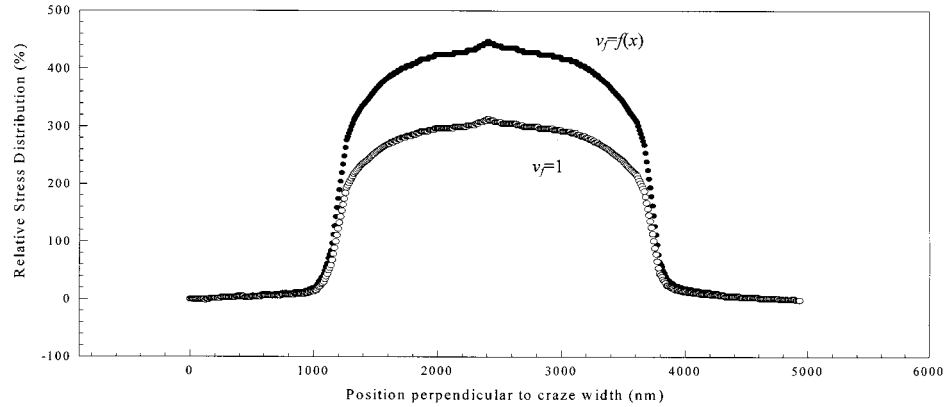

Figure 4. Stress distribution in the craze.

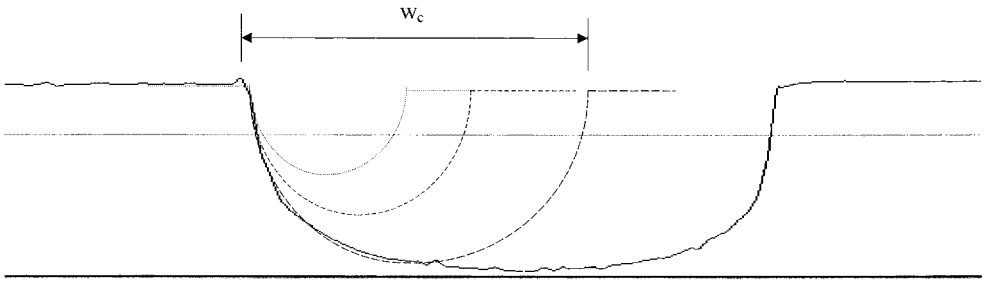

Figure 5. Neck development during craze widening. The critical craze width w_c is the width above which the craze necking becomes mature.

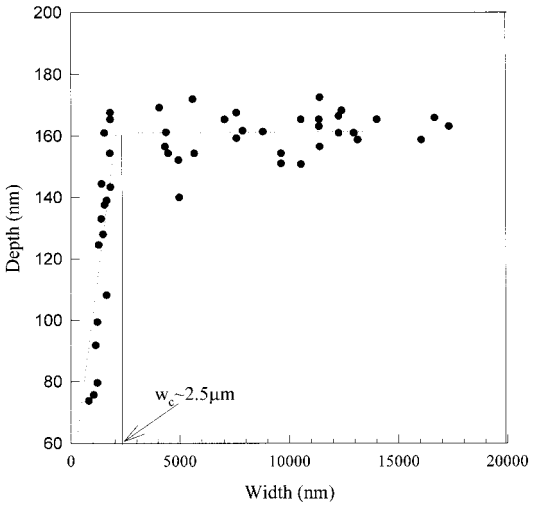

Figure 6. Maximum depth vs craze with in a 0.45 μm thick PS film.

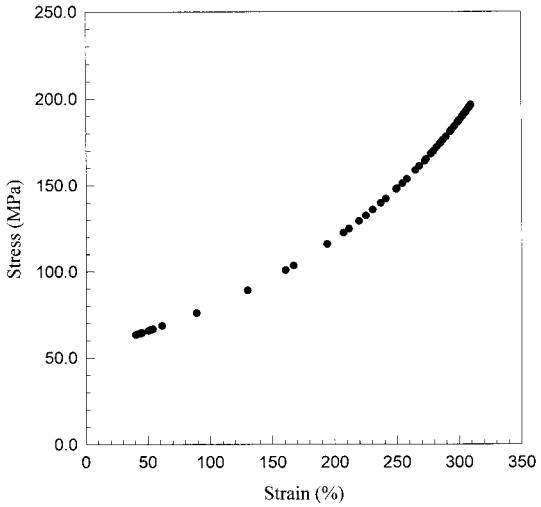

Figure 7. Stress−strain curve of fibril drawing in a 0.45 μm PS film (craze width = 2700 nm).

strain curve of the craze because of the multiple formation of crazes in the specimen. By combining the strain and stress calculated above, the stress−strain curve of craze fibrillation can be constructed. Before carrying out this process, it was noticed that the AFM topographic profile of the shoulder zone near the craze boundary was followed by crazes of different widths. The schematic profiles of a widening craze are shown in Figure 5. Corresponding to the profiles in Figure 5, the craze depth vs craze width is shown in Figure 6. The depth of the craze depression was observed to increase linearly with width when craze depth is less than the critical width w_c. When the craze widens beyond w_c, ca. 2.5 μm for a 0.45 μm thick PS film as shown in Figure 6, the depth becomes constant with craze width. When the polymer is drawn into a craze, the film first undergoes a neck formation which generates the contour of the shoulder zone at the boundary of the craze. When the shoulder formation is completed at the critical craze width, neck propagation initiates, generating the plateau region within the craze depression. This is the so-called micronecking process of glassy polymers.[22]

Apparently, the stress vs strain data during the shoulder zone formation are critical for the understanding toward the craze fibrillation process. Figure 7 shows a stress vs strain curve of crazing, constructed by combining the strain and the stress calculated above from a corrected AFM topographic profile. This curve represents the stress−strain curve of the polymer craze fibrillation process. The deformation strain of crazing starts from the critical strain for crazing, ca. 1%, to 300% at the central neck region. In the central neck region of the craze, the depth is nearly constant, resulting unvarying local strain and stress values.

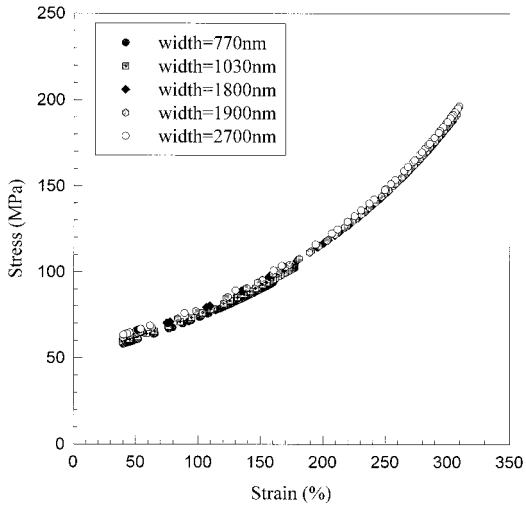

Figure 8. Stress−strain curves of fibril drawing to different width.

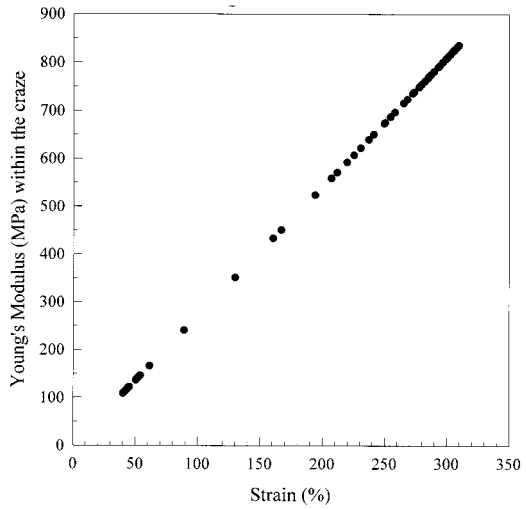

Figure 9. Young's modulus within the craze as a function of fibril drawing.

Figure 8 also shows the stress−strain for different craze widths. Apparently, the microdrawing process of crazing consistently follows a single master curve.

The ratio of the stress and the strain represents the modulus of the materials. From the slope of the stress−strain curve of crazing, the variation of the Young's modulus during the formation of craze can be obtained. This result is shown in Figure 9. It is worthy noting that craze initiation is generally believed to result from local strain softening. During the incipient growth of crazes,[1,4] the local sites of craze initiation were assumed to become rubbery. Once the softened polymer is drawn into crazes, it soon hardens due to chain orientation. As shown in Figure 9, the modulus increases steadily during craze fibrillation and finally reaches a maximum when craze width approaches w_c, the onset of craze neck propagation. Greater modulus values at the neck than that in the shoulder regions indicate that craze widens by drawing new materials into the craze instead of material creeping within the craze. This is consistent with Kramer's previous conclusions from TEM observation.[1,16−19] Furthermore, the strain hardening rate can be readily obtained from the craze stress−strain curve shown in Figure 10. The strain hardening rate increases rapidly at the craze boundaries and then

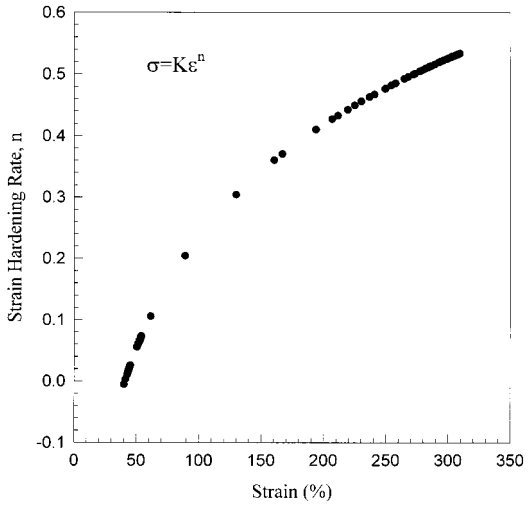

Figure 10. Strain hardening rate vs local strain during craze microdrawing in PS thin films.

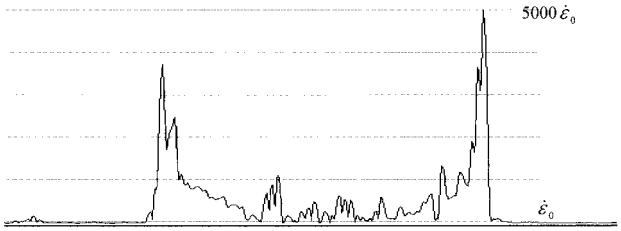

Figure 11. Local strain rate distribution across the craze width within a craze.

saturates to a maximum at the neck region. Therefore, during the craze drawing process, the drawn polymer in the craze becomes harder and harder to draw further. When drawn polymer finally reaches the neck region, the deformation virtually ceases.

The strain localization causing the heterogeneous plastic deformation is a result of the nonuniform strain rate distribution during deformation. The strain rate distribution in the crazed region can be calculated from the AFM topographic data by following the approach adopted by G'sell and Marquez-Lucero.[33] They used the necking theory of Hutchinson and Neale[34] for treating the problem of a steady-state neck propagation. By the conservation of volume during deformation, the strain rate distribution at any point in the neck can be expressed as[33]

$$\dot{\epsilon}(x) = -k_p\{\exp[\epsilon(x) - \epsilon_0]/t(x)\}\left[\frac{\partial t(x)}{\partial x}\right]$$

where k_p is the constant neck propagation speed and ϵ_0 represents the strain outside the craze. Since the necking model of G'sell and Marquez-Lucero assumes a constant velocity of neck propagation, only mature crazes with a width greater than the critical craze width w_c were studied using this approach. The calculated strain rate distribution in the craze is shown in Figure 11. The shoulder region at the craze/matrix boundary is the mostly rapidly strained region during the propagation of necked area. The strain rate at the shoulder zone is approximately 3 orders of magnitude greater than that in the regions away from the shoulder. The strain rate elsewhere is much slower.

The local strain rate information within a craze can be further utilized to investigate the microdrawing

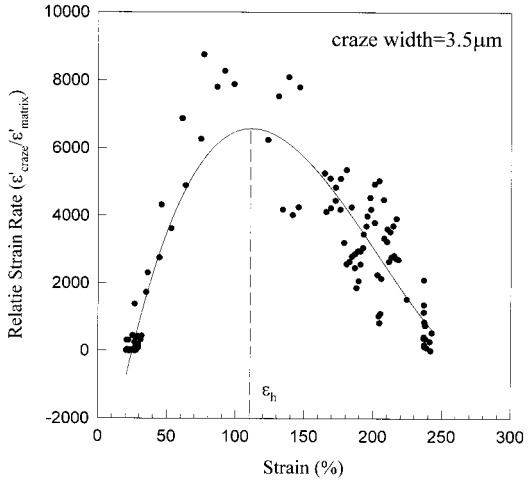

Figure 12. Local strain rate as a function of fibril drawing in the craze.

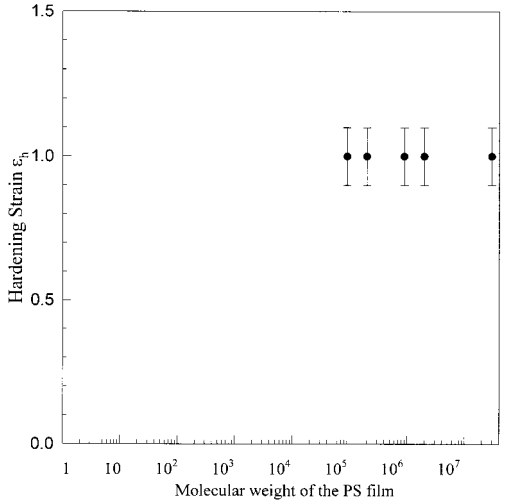

Figure 13. Hardening strain ϵ_h vs molecular weight of the PS film.

process of craze fibrillation. Figure 12 shows how the local strain rate of the drawn polymer varies with strain during crazing. In this figure, two microdrawing curves are overlapped due to the fact that each craze has two boundaries, and at each boundary a microdrawing process is taking place. The full range of the drawing strain starts from the crazing strain, ca. 1%, to the plateau strain at the central region of craze. The strain rate increases as the material is drawn into the site of the strain localization. This means that the material deformation was accelerated during the straining due to an apparent strain softening. The molecular mechanisms of strain softening at this deformation stage, however, are not clear. As the strain increases, the strain rate peaks and then decreases to a level corresponding to strain hardening of the necking process. The decline of the strain rate can be attributed to the strain hardening of the polymer in the craze. This is consistent with the observation that the modulus within the craze increases with drawing strain as shown in Figure 9. The strain with the maximum strain rate signifies the beginning of strain hardening and therefore is termed the hardening strain ϵ_h. The value of the hardening strain ϵ_h should be related to the molecular entanglement network structure, and a further experiment was carried out to explore this possible relationship.

IV. Effect of Entanglement Network Structure. From the basic affine deformation model of polymer, it is assumed that the end-to-end vectors joining the chemical or physical cross-linking point deform "uniformly". The chain is free to assume a random configuration between these points. During the deformation of the polymer network, it is the entanglement points that sustain and transfer the deformation to the network. The entanglement density of the polymer network can be calculated from the rubber elastic theory to be[1,21,31]

$$\nu_e = \rho N_A / M_e$$

ρ is the density of the polymer, N_A is Avogadro's number, and M_e is the entanglement molecular weight. The root-mean-square end-to-end distance between entanglement points in the network is $d = k(M_e)^{1/2}$. The theoretical maximum extension ratio of a single strand in the polymer entanglement network λ_{max} can be expressed as[1,21,31]

$$\lambda_{max} = l_e / d$$

where l_e is the average contour length between two adjacent entanglement points and can be approximated as $l_e = l_0 M_e / M_0$ in which l_0 and M_0 are the length and molecular weight of the building units of the chain. The correlation of λ_{max} and entanglement density ν_e can therefore be simplified as

$$\lambda_{max} = A / \sqrt{\nu_e}$$

It is clear from this relationship that the larger the entanglement density, the lower the λ_{max} if no chain scission or disentanglement takes place during crazing. In the initial stage of craze formation, as shown in Figure 12 the strain rate increases as a result of the deformation of the chain network. Although the apparent strain softening mechanisms are not clear, it is plausible that at the strain localization sites the glassy polymer chains are activated by the large and concentrated mechanical energy. This enables the chains to undergo a higher degree of motions such as rotations and large vibrations. Under the influence of the applied deformation, the locally activated polymer network deforms in the direction of the external strain. The deformation of the local chain network, however, should be limited by the intrinsic entanglements. At a certain point of deformation, the motion of the chain eventually slows. This point should correspond to the hardening strain ϵ_h defined previously. Therefore, ϵ_h must be linearly proportional to λ_{max}. Consequently, polymer blends of lower entanglement density that have been shown to have a greater λ_{max} produce a greater ϵ_h value. Therefore, we investigated the strain rate distribution of different molecular weight PS's as well as the PS's of different entanglement density. To compare with the ductile deformation mode of local shearing, PPO blended with low molecular PS was also studied.

To investigate the effect of molecular weight, PS films of several molecular weights were prepared, from which the strain rate distribution within the craze of each sample was obtained. The hardening strain ϵ_h in crazes of different molecular weight is shown in Figure 13. It

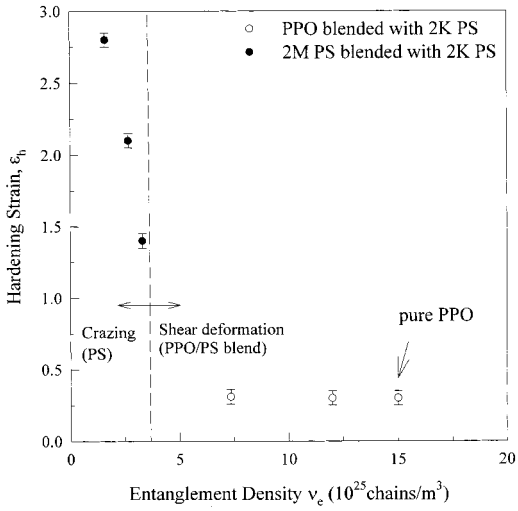

Figure 14. Hardening strain ϵ_h vs the entanglement density of the PS film.

is evident that molecular weight in the range from 90K to 20M at room temperature triggers no significant effect.

The relationship between the hardening strain ϵ_h and the entanglement density is shown in Figure 14. The variation of entanglement density is achieved by blending the PPO or 2M PS with low molecular weight PS (M_w = 2K). The entanglement density of pure PPO is 15×10^{25} and 3.3×10^{25} chains/m^3 in the pure 2M PS. Since low molecular weight 2K PS is far below the entanglement molecular weight of PS, 19K, blending with 2K PS will dilute the molecular network and decrease the entanglement density of the polymer blend. The dilute entanglement density[21] can be expressed as

$$\nu = \nu_e \chi^2$$

where ν is the effective entanglement density after blending, ν_e is the entanglement density of the high molecular weight polymer, and χ is the fraction of the high molecular weight polymer. It is demonstrated that, for the polymer blend with higher entanglement density, the hardening strain ϵ_h is very low and around 0.3, independent of the variation in entanglement density. However, for the polymer blend with low entanglement density, the hardening strain ϵ_h increases remarkably from 1.4 to approximately 2.8 as entanglement density decreases from the $\nu_e = 3.3 \times 10^{25}$ chains/m^3 (the undiluted 2M PS) to 1.62×10^{25} chains/m^3 (30% diluted with 2K PS) following the $1/\sqrt{\nu_e}$ dependence. It is important to note that the samples with the hardening strain ϵ_h independent of ν_e are ductile polymers that, upon stretching, undergo local shear deformation rather than crazing. On the other hand, those low-ν_e samples in which ϵ_h decreases in consistency with the $1/\sqrt{\nu_e}$ dependence are the craze-forming brittle polymers. Clearly, although the ductile and brittle glassy polymers both deform by the similar micronecking mechanism[22,23] in the microscopic terms, i.e., local shear deformation or crazing, the varying dependence of ϵ_h on ν_e clearly demonstrates the critical difference between these two strikingly different deformation modes of glassy polymers.

From Figure 14, it is clear that the polymer with a loose entanglement network structure tends to undergo the brittle crazing process upon applied strain. This is consistent with Kramer's previous results.[1] In this low entanglement density regime, however, the hardening strain ϵ_h increases with the distance between entanglements, indicating mobile molecular segments between entanglements during crazing. It is reasonable to state that the externally applied strain is more likely to localize in polymers of this certain type of entanglement network. When strain localizes, polymers will deform in a brittle manner until fracture subsequently sets in. On the contrary, for ductile polymers that undergo local shear deformation upon stretching, the ϵ_h is very low and independent of the distance between entanglements. This observation indicates a tight and "rigid" entanglement network that, upon external deformation, tends to delocalize the deformation to a larger area, effectively reducing the loading on each load-bearing strand of the entanglement network, hence demonstrating ductile behavior.

4. Conclusions

1. The crazing of PS thin film is a result of the micronecking mechanism. The strain and stress distribution of the craze in the transversal direction can be analyzed from the AFM scanned profile by the Bridgman plasticity model.

2. The stress−strain curve of the drawing of craze fibrils during crazing can be obtained by combining the calculated strain and stress from the craze topographic profile. The curve shows evident strain hardening during the formation of crazes.

3. Crazing is a consequence of strain localization, as evident from the heterogeneous distribution of strain rate in a craze. The maximum strain rate is located at the boundary of the craze. This conclusion is consistent with the previous surface drawing model for crazing proposed by Kramer.[1,16−19]

4. The strain rate distribution within a craze can be obtained to further investigate the microdrawing process of craze fibrillation. The strain rate increases as the material is drawn into the site of the strain localization, indicating an apparent strain softening in the initial stage of craze fibrillation. As the strain increases, the strain rate peaks and then decreases to a level corresponding to strain hardening of the necking process. The decline of the strain rate is caused by the strain hardening of the polymer in the craze. The strain with the maximum strain rate signifies the beginning of strain hardening and therefore is termed the hardening strain ϵ_h.

5. The hardening strain ϵ_h is independent of the molecular weight of PS from 90K to 20M at room temperature. However, the hardening strain ϵ_h decreases with increasing entanglement density in the craze-forming regime. Yet when the deformation mode switches from crazing to local shear yielding as the entanglement density becomes higher than a threshold value, ϵ_h becomes independent of entanglement density.

6. In the craze-forming regime, the hardening strain ϵ_h increases with the distance between entanglements, implying the presence of mobile molecular segments between entanglements during crazing. Hence, the externally applied strain is considered more likely to localize, and the polymer deforms in a brittle manner of crazing. On the other hand, the ductile polymers undergo local deformation with a very low hardening strain ϵ_h which is independent with the distance between entanglements, indicating a tight and "rigid"

entanglement network that tends to delocalize the deformation to a larger area.

Acknowledgment. The authors acknowledge the financial support from National Science Counsel. The continuing software support provided by Mr. I. C. Yang, the author of the AFMREAD program used here for AFM data analysis, is greatly appreciated.

References and Notes

(1) Kramer, E. J. *Adv. Polym. Sci.* **1983**, *52/53*, 1.
(2) Sternstein, S. S.; Myers, F. A. *J. Macromol. Sci., Phys.* **1973**, *B8*, 557.
(3) Argon, A. S.; Hannoosh, J. G. *Philos. Mag.* **1977**, *36*, 1195.
(4) Gent, A. N. In *The Mechanics of Fracture, AMD;* Erdogon, F., Ed.; ASME: New York, 1976; Vol. 19, p 55.
(5) LeGrand, D. G.; Kambour, R. P.; Haaf, W. R. *J. Polym. Sci., Part A-2* **1972**, *10*, 1565.
(6) Kitagawa, M. *J. Polym. Sci., Polym. Phys.* **1976**, *14*, 2095.
(7) Argon, A. S.; Salama, M. M. *Mater. Sci. Eng.* **1977**, *23*, 219.
(8) Steger, T. R.; Nielsen, L. E. *J. Polym. Sci., Polym. Phys.* **1978**, *16*, 613.
(9) Lauterwasser, B. D.; Kramer, E. J. *Philos. Mag.* **1979**, *A39*, 469.
(10) Brown, H. R. *J. Mater. Sci.* **1979**, *14*, 237.
(11) Farrar, N. R.; Kramer, E. J. *Polymer* **1981**, *22*, 691.
(12) Donald, A. M.; Kramer, E. J. *Philos. Mag.* **1981**, *A43*, 857.
(13) Wang, W.-C. V.; Kramer, E. J. *J. Mater. Sci.* **1982**, *17*, 2013.
(14) Takahashi, K.; Hyodo, S. *J. Macromol. Sci., Phys.* **1981**, *B19*, 695.
(15) Kawagoe, M.; Kitagawa, M. *J. Polym. Sci., Polym. Phys.* **1981**, *19*, 1423.
(16) Donald, A. M.; Kramer, E. J. *Polymer* **1982**, *23*, 457.
(17) Donald, A. M.; Chan, T.; Kramer, E. J. *J. Mater. Sci.* **1981**, *16*, 669.
(18) Yang, A. C.-M.; Kramer, E. J. *J. Polym. Sci., Polym. Phys. Ed.* **1985**, *23*, 1353.
(19) Yang, A. C.-M.; Kramer, E. J.; Kuo, C. C.; Phoenix, S. L. *Macromolecules* **1986**, *19*, 2010.
(20) Yang, A. C.-M.; Kramer, E. J.; Kuo, C. C.; Phoenix, S. L. *Macromolecules* **1986**, *19*, 2020.
(21) Kramer, E. J.; Berger, L. L. *Adv. Polym. Sci.* **1990**, *91/92*, 1.
(22) Yang, A. C.-M.; Kunz, M. S.; Logan, J. A. *Macromolecules* **1993**, *26*, 1767.
(23) Yang, A. C.-M.; Wang, R. C.; Kunz, M. S.; Yang, I. C. *J. Polym. Sci., Polym. Phys. Ed.* **1996**, *34*, 1141.
(24) Taylor, G. I. *Proc. R. Soc. London* **1950**, *A201*, 192.
(25) Saffman, P. G.; Taylor, G. I. *Proc. R. Soc. London* **1958**, *A245*, 312.
(26) Fields R. J.; Ashby, M. F. *Philos. Mag.* **1976**, *33*, 33.
(27) Bilby, B. A.; Eshelby, J. D. Dislocation and the Theory of Fracture. In *Fracture;* Liebowitz, H., Ed.; Academic Press: New York, 1972; Vol. 1, Chapter 2, p 111.
(28) Porod, G. *Kolloid Z.* **1952**, *125*, 51, 109.
(29) Parades, E.; Fisher, E. W. *Makromol. Chem.* **1979**, *180*, 2707.
(30) Bridgman, D. W. *Studies in Large Plastic Flow and Fracture*; Harvard University Press: Cambridge, 1964; p 9.
(31) Ward, I. M. *Mechanical Properties of Solid Polymers*, 2nd ed.; John Wiley & Sons Press: New York, 1983.
(32) Dieter, G. E. *Mechanical Metallurgy;* McGraw-Hill: New York, 1988.
(33) G'sell, C.; Marquez-Lucero, A. *Polymer* **1993**, *34*, 2740.
(34) Hutchinson, J. W.; Neale, K. W. *J. Mech. Phys. Solids* **1983**, *31*, 405.

MA001367R